ACS OMEGA

http://pubs.acs.org/journal/acsodf

Article

From Topological Nodal-Line Semimetal to Insulator in ABW-Ge_4: A New Member of the Germanium Allotrope

Yuxin Zou, Ningjun Wu, Tielei Song, Zhifeng Liu, and Xin Cui*

Cite This: *ACS Omega* 2023, 8, 27231−27237

Read Online

ACCESS | Metrics & More | Article Recommendations | Supporting Information

ABSTRACT: Topological semimetals have attracted much attention because of their excellent properties, such as ultra-high speed, low energy consumption quantum transport, and negative reluctance. Searching materials with topological semimetallic properties has become a new research field for Group-IV materials. Herein, using first-principles calculations and tight-binding modeling, we proposed a topological nodal-line semimetal ABW-Ge_4 when spin−orbit coupling (SOC) is ignored, which is composed of pure germanium atoms in a zeolite framework ABW. It holds excellent dynamic and thermal stability. In its electronic band structure, there exists a stable Dirac linear band crossing near the Fermi energy level, which forms a closed ring in the $k_x = 0$ plane of the Brillouin zone (BZ). Our symmetry analysis reveals that the nodal ring is protected by M_x mirror symmetry. Furthermore, by examining the slope index in all possible $\boldsymbol{k}$ paths through the considered Dirac point, we find that the band dispersion near the Dirac point is greatly anisotropic. In some direction, the Fermi velocity is even larger than that of graphene, being promising for the future ultra-high speed device. When spin−orbit coupling is included, the nodal line is gapped and the system becomes a topological insulator with topological invariants $Z_2 = 1$. Our findings not only identify a new Ge allotrope but also establish a promising topological material in Group-IV materials, which may have the desirable compatibility with the traditional semiconductor industry.

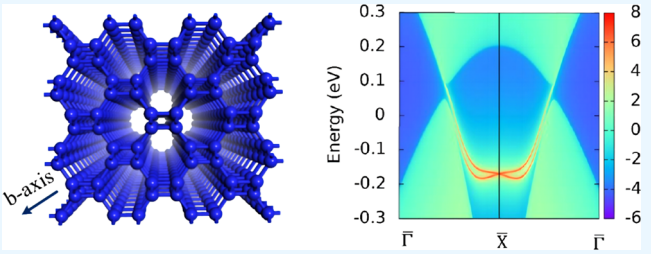

1. INTRODUCTION

As is known, the Group-IV elemental solids (e.g., silicon and germanium) are quite important in semiconductor and microelectronics industries, which have been extensively studied.[1] Owing to the complex potential energy surface, the Group-IV elements can form various allotropes with different structural and electronic properties, which provides promising platforms for constructing multifunctional microelectronic devices. Hence, the searching for stable Group-IV allotropes has attracted considerable attention from both theoretical and experimental researchers.[2−5] However, these studies mainly focus on carbon (C) and silicon (Si), and the studies about germanium (Ge) allotropes are relatively few. The most prominent Ge allotrope is the diamond-cubic Ge, denoted as dc-Ge, which has higher electron and hole mobilities, and smaller indirect band gap with respect to that of dc-Si.[6] In addition to dc-Ge, the high-pressure transitions of Ge allotropes have already been confirmed by many experimental works, via using the compression or subsequent decompression on dc-Ge.[7−10] For instance, under 10.6 ± 0.05 GPa compression, the dc-Ge will transform into a body-centered tetragonal Ge (β-Sn-Ge);[7] then, the β-Sn-Ge can further transform into a tetragonal phase ($P4_32_12$-Ge) at 7.6 ± 0.05 GPa during the slow release of pressure; orthorhombic symmetry *Imma* Ge (*Imma*-Ge) is found to exist above ∼75 GPa;[8] the β-Sn-Ge structure can transform into a simple hexagonal (sh-Ge) phase at 75 ± 3 GPa and to a double hexagonal close-packed structure (dhcp-Ge) at 102 ± 5 GPa.[10]

In 2011, the new Ge phase *m*-allo-Ge was synthesized from Li_7Ge_{12},[11] which was confirmed to have a direct band gap. The bulk phase of ST12-Ge was synthesized in 2017,[12] and its optical measurements indicate that it is a semiconductor with an indirect band gap of 0.59 eV. ST12-Ge is confirmed to be a better material for infrared detection compared with the dc-Ge and has potential applications in both high-frequency and low-voltage electronics. Additionally, Tang et al. synthesized a new well-crystallized metastable phase Ge(oP23-Ge) by adjusting the properties of ionic liquids in 2018.[13] It is proved that oP23-Ge is a diamagnetic semiconductor with a narrow direct optical band gap (E_g) of 0.33 eV.

In recent years, with the improvement of computer performance and algorithms, more and more studies based on first-principles calculations are devoted to predict the new Ge phase with interesting properties. Nguyen et al. proposed a

Received: April 14, 2023
Accepted: July 4, 2023
Published: July 18, 2023

https://doi.org/10.1021/acsomega.3c02542
ACS Omega 2023, 8, 27231−27237

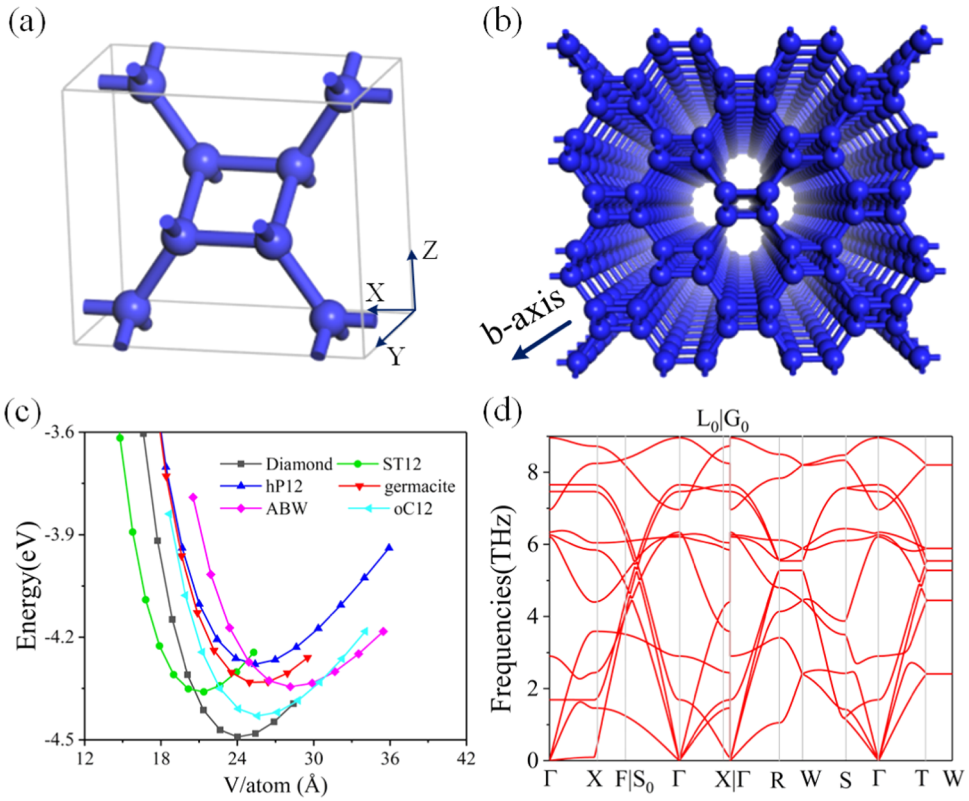

Figure 1. (a) Unit cell of the optimized structure of ABW-Ge_4. (b) Perspective view from the crystallographic *b*-axis. (c) Total energy as a function of volume per Ge atom for ABW-Ge_4 in comparison with some known germanium allotropes. (d) Calculated phonon dispersion curves of ABW-Ge_4.

new dynamically stable Ge allotrope with a distorted sp^3 hybrid framework in $P4_2/mnm$ symmetry.[14] Their band-structure calculations show that the $P4_2/mnm$ Ge is semiconducting with an energy gap close to the optimal value for optoelectronic or photovoltaic applications. Using ab initio method, Saleev et al. predicted six new allotropes of Ge. Their structural, elastic, vibrational, electronic, and optical properties have been systematically studied.[1] The results show that one of the Ge allotropes has a very small band gap, in agreement with the semimetallic nature of amorphous Ge. It is worth mentioning that Cao et al. predicted a metastable allotrope of Ge (named germancite) in 2016,[15] which is constructed by the known staggered layered dumbbell (SLD) structures. Interestingly, it is found that germancite is a Dirac semimetal with a pair of Dirac points on the screw axis. Moreover, the quantum thin film of germancite is confirmed to be an intrinsic quantum spin Hall insulator. However, investigations on topological semimetals (TSMs) composed of the Ge element are far from complete. And whether the properties of topological semimetals can be preserved with the rotational symmetry being broken? In this context, one naturally wants to know whether there exist topological nodal-line semimetals in Ge, similar to those in carbon and silicon, and what happens to the TSM behavior when spin−orbit coupling (SOC) is included.

In fact, the study of topological semimetals has become a hot topic in both condensed matter physics and materials science. Wang et al. theoretically predicted that both A_3Bi (A = Na, K, Rb)[16] and Cd_3As_2[17] were three-dimensional (3D) Dirac semimetals, which were then experimentally confirmed in just a few years.[18] This makes the research of topological materials a hot field. In physics, the distinct feature of topological semimetals is the existence of topologically stable linear crossing near the Fermi level.[19] So far, various topological semimetals have been identified, and their species are becoming more and more diverse according to the degeneracy of the nodes, the distribution of the nodes in BZ space, and the feature of band dispersion. The known topological semimetals include Weyl semimetal,[20−22] nodal-line semimetals,[23−25] Dirac semimetal,[15,16,26] etc. Specifically, when the Dirac or Weyl nodes form a one-dimensional (1D) continuous line, the corresponding materials should be nodal-line semimetals;[27] furthermore, they can be divided into type I and II topological semimetals according to the feature of band dispersion. Owing to the novel physical properties of topological nodal semimetals, such as high carrier mobility and superconducting phenomena, they have promising applications in next-generation electronic devices.

However, TSMs possessing a nodal ring could be driven into topological insulators (TIs) when SOC is included.[28,29] TI is a special insulator with robust surface state for a 3D system. The common feature between TSMs and TIs is that the nodal ring from the crossing between the conduction band and the valence band is protected by the reflection symmetry and the time-reversal symmetry, and SOC plays a significant role in driving the quantum-phase transition from TSM into TI. Based on first-principles calculations, Zhu et al. found a TSM phase in Ba_2X (X = Si, Ge) with a nodal ring in the k_x = 0 plane, which would evolve into the TI phase by SOC.

In this paper, on the basis of first-principles calculations, we identify a new stable Ge allotrope, which holds a similar framework of the Zeolite structure of ABW, termed as ABW-

https://doi.org/10.1021/acsomega.3c02542
ACS Omega 2023, 8, 27231−27237

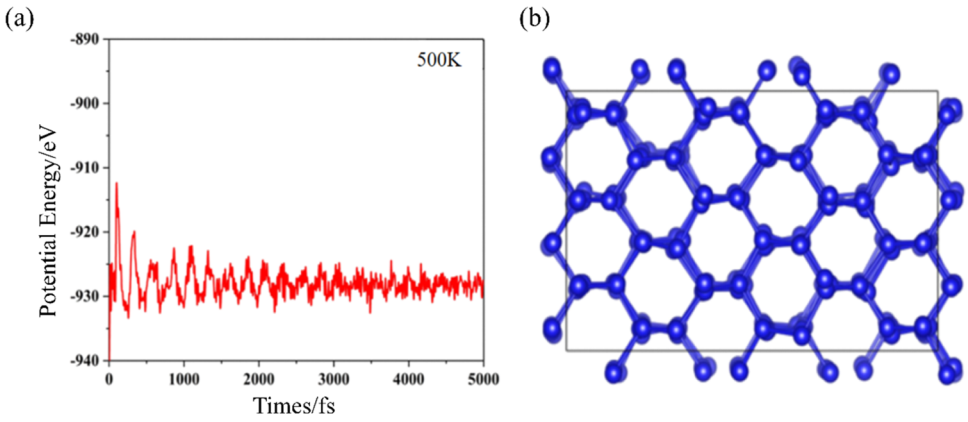

Figure 2. (a) Fluctuation of potential energy during 5000 fs FPMD simulation for ABW-Ge_4 at 500 K. (b) Snapshot structure of ABW-Ge_4 after molecular dynamics simulation for a 3 × 3 × 3 supercell.

Ge_4. From the electronic band calculations, we find that there exist band inversion and Dirac linear crossing in the vicinity of the Fermi level. Specifically, the Dirac nodes can form a closed nodal loop on the k_x = 0 plane of symmetric space and protected by a mirror symmetry. In other words, ABW-Ge is a typical topological nodal-line semimetal without SOC. Furthermore, the anisotropy of the low-energy band around some considered Dirac point is discussed. Moreover, when considering SOC, a topological phase transition from nodal-loop semimetals to topological insulator occurs and is characterized by calculating surface states. Our work not only fills the gap in topological semimetals in germanium isomorphic phases but also finds topological phase transitions whose topological electronic properties are expected to be applied in future high-speed electronic devices.

2. COMPUTATIONAL METHODS

Our density functional theory (DFT)[30] calculations with projector-enhanced wave (PAW)[31] are implemented in Vienna Ab initio Simulation Package (VASP).[32] The generalized gradient approximation (GGA) in the form of Perdew–Burke–Ernzerhof (PBE) is used to treat the exchange–correlation interactions.[33] A plane-wave basis set with a kinetic energy cutoff of 500 eV is used. By using Monkhorst–Pack methods, the k point meshes with a uniform density of $2\pi \times 0.02$ $Å^{-1}$ are adopted to sample the reciprocal BZ. The forces on ions are calculated according to the Hellmann–Feynman theorem.[34] In the case of complete relaxation, the convergence thresholds of total energy and ionic force components are set to 1×10^{-8} eV and 10^{-3} eV/Å, respectively. The phonon frequencies are obtained using the finite displacement method, which is implemented in PHONOPY code.[35] In the first-principles molecular dynamics (MD) simulations, the system is established with a 3 × 3 × 3 supercell containing 216 germanium atoms. The temperature is set to 500 K. The nodal lines and surface states are calculated using WannierTools package,[36] where the Wannier90 code is built based on the Wannier tight-binding model.[37]

3. RESULTS AND DISCUSSION

Figure 1 shows the crystal structure of ABW-Ge_4. The space group is *Imma* (no. 74), which has many symmetry operations, including C_2 rotation axis, central inversion operation, and M_x mirror symmetry. The time-reversal symmetry of ABW-Ge_4 is retained as it has nonmagnetic properties. The results of the optimized lattice parameters of ABW-Ge_4 are a = 7.91 Å, b = 4.14 Å, and c = 6.92 Å, respectively. There are four atoms in a primitive cell, and there is only one nonequivalent germanium atom, taking the Wyckoff coordinates of 8i (0.16, 1.25, 0.10). As one can see from Figure 1b, ABW-Ge_4 has a porous structure and this suggests that it might be synthesized experimentally by the high-pressure method like *Imma* Ge.[8] In this regard, the stability of the porous structure ABW-Ge_4 must be of particular concern.

To investigate the energy stability of ABW-Ge_4, the total energy of ABW-Ge_4 as a function of volume per atom is calculated. For comparison, the results of five known Ge allotropes, including dc-Ge, ST12, hP12, oC12, and germancite structures, are also presented (see Figure 1c). The results show that the average energy per atom of ABW-Ge_4 in the equilibrium state is 0.16 eV higher than that of *dc*-Ge, but it is slightly lower than that of the Dirac semimetallic phase (germancite) predicted by Cao et al.[15] and greatly lower than that of the hP12 phase. This means that the proposed ABW-Ge_4 is competitive in energy stability with respect to the known allotropes.

The dynamic stability of ABW-Ge_4 has been confirmed by phonon dispersion calculation. Figure 1d shows the phonon dispersion in the first BZ along typical high-symmetry points and high-symmetry directions of ABW-Ge_4. It can be observed that calculated phonon dispersion curves do not contain soft modes, i.e., negative frequencies, in any highly symmetric direction. This indicates that ABW-Ge_4 is dynamically stable under ambient pressure.

Furthermore, in order to investigate the mechanical stability of this porous structure, we have also calculated the elastic constants of ABW-Ge_4. The values of independent elastic constants C_{11}, C_{12}, C_{13}, C_{22}, C_{23}, C_{44}, C_{55}, and C_{66} of ABW-Ge_4 are 79, 35, 51, 110, 29, 34, 46, and 30 GPa, respectively, which are in good accordance with the Born mechanical stability criterion, namely,

$$C_{11} > 0,\ C_{11} \times C_{22} > C_{12}^2$$

$$C_{11} \times C_{22} \times C_{33} + 2C_{12} \times C_{13} \times C_{23} - C_{11} \times C_{23}^2 - C_{22} \times C_{13}^2 - C_{33} \times C_{12}^2 > 0$$

$$C_{44} > 0,\ C_{55} > 0,\ C_{66} > 0$$

https://doi.org/10.1021/acsomega.3c02542
ACS Omega 2023, 8, 27231−27237

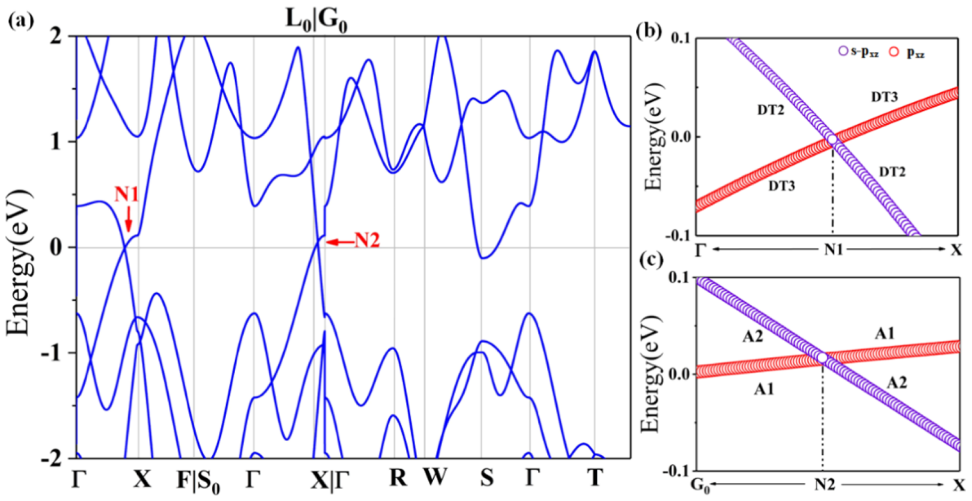

Figure 3. (a) Electronic band structure of ABW-Ge_4 without SOC. Orbital projections near (b) N1 and (c) N2. DT2, DT3 and A1, A2 represent irreducible representations of the intersection bands near the nodes N1 and N2, respectively.

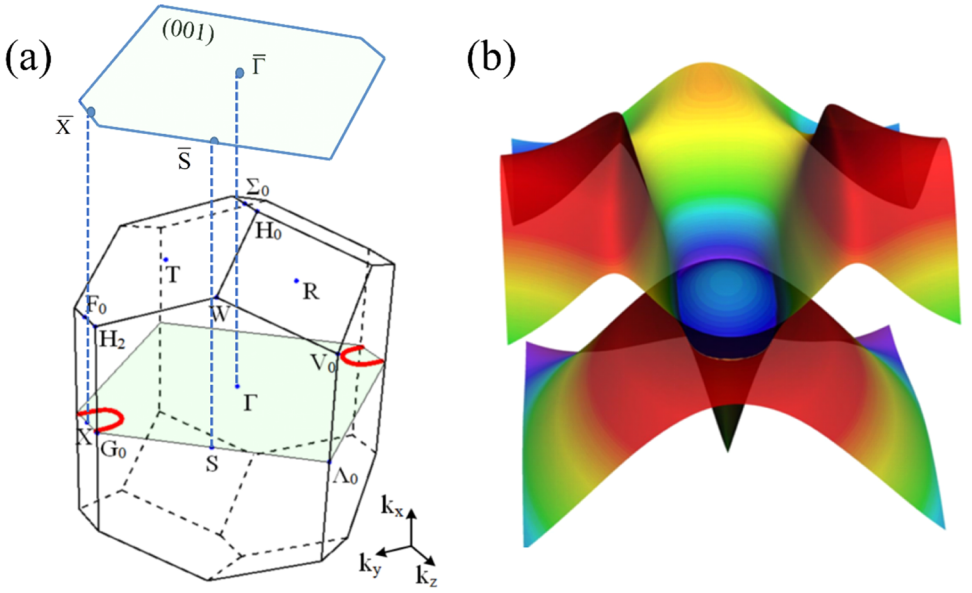

Figure 4. (a) High symmetry points and representation of nodes in Brillouin zone. (b) The three-dimensional and energy band of the plane where the node line is located.

Therefore, ABW-Ge_4 is also mechanically stable.

To further explore the thermal stability, we performed first-principles molecular dynamics (FPMD) simulation by building a 3 × 3 × 3 supercell with 108 Ge atoms at 500 K. Figure 2a shows that the average total potential energy of ABW-Ge_4 remains almost constant during the whole simulation time period ranging from 0 to 5 ps. As shown in Figure 2b, no structural collapse can be found in ABW-Ge_4 after heating for more than 5 ps. So ABW-Ge_4 can be thermally stable up to 500 K, which is larger than the room temperature for practical application.

The electronic band structure of ABW-Ge_4 without SOC is shown in Figure 3. It can be seen that there are two Dirac linear crossings (denoted as N1 and N2) between the valence and conductance bands along the Γ−X and G_0−X paths near the Fermi level, marked as points N1 and N2, respectively. As is known, the band crossing of most topological semimetals comes from band inversion. To examine the feature of band inversion, we calculated the orbital and atom-decomposed band structures, as illustrated in Figure 3b. The red and purple lines denote p_{xz} and $s + p_{xz}$ states, respectively. We can see that from Γ to N1 point, the energy of the p_{xz} state is lower than that of the $s + p_{xz}$ state, while from the N1 to X point, the energy ordering between p_{xz} and $s + p_{xz}$ states is changed and the energy band reversal occurs. Similar orbital projection features also appear near the N2 point. In order to explore the origin of band inversion from symmetry, we calculated the eigenvalues of symmetric operators near crossing points. The irreducible representations of the crossing band subgroups at the N1 point (along the Γ−X path) are denoted as DT2 and DT3, while A1 and A2 are the crossing band subgroups around the N2 point (along the G_0−X path). According to these irreducible representations, we further confirm that they all correspond to the characteristic wave functions of M_x mirror reflection. This indicates that the band inversion in ABW-Ge_4 is caused or protected by the mirror reflection symmetry.

In momentum space, mirror reflection symmetry can be defined as M_x:M_x $[(k_x, k_y, k_z) \rightarrow (-k_x, k_y, k_z)]$. Symmetry can

https://doi.org/10.1021/acsomega.3c02542
ACS Omega 2023, 8, 27231−27237

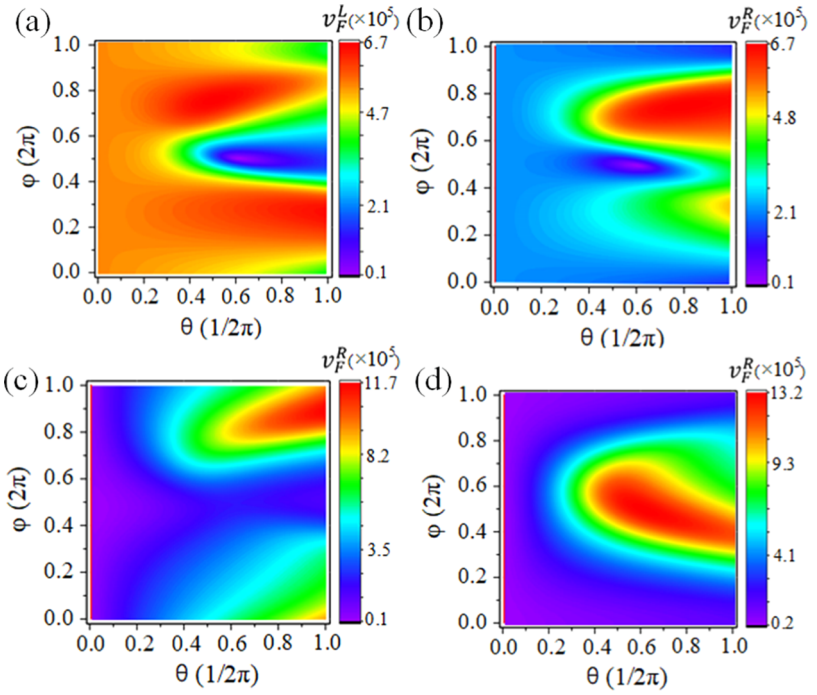

Figure 5. (a) Schematic diagram of the spherical coordinates in the momentum space with node N1 as the origin. (b) Node N1 representation in the spherical coordinates in the BZ. Slope indices (c) γ^{L} and (d) γ^{R} of node N1 along all possible k directions (θ, φ).

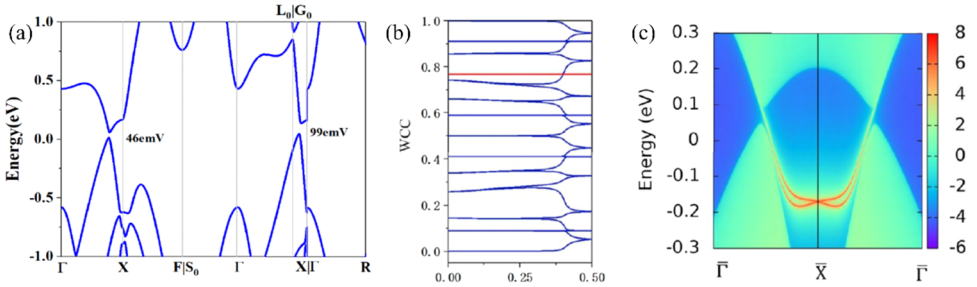

Figure 6. (a) Electronic band structure of ABW-Ge_4 under SOC. (b) Z_2 topology invariants calculated based on Wannier charge centers algorithm under SOC. (c) The semi-infinite (100) edge state of ABW-Ge_4.

be used as a unitary operator representation for one electron wave function, satisfying $M_x^2 = (-1)^{2S}$, where S is the spin of a single particle. When the SOC does not exist, the system can be considered as a spin-free system ($S = 0$) that maintains complete SU (2) spin rotation symmetry, and M_x has two eigenvalues 1 and −1, respectively. When the non-interacting system described by Hamiltonian H (k_x, k_y, k_z) has a mirror reflection symmetry M_x, there exists M_xH (k_x, k_y, k_z) $M_x^{-1} = H$ ($-k_x$, k_y, k_z). It can be seen that on the two high symmetry planes of the BZ, i.e., $k_x = 0$ and $k_x = \pi$, mirror operators and Hamiltonians have the same eigenstates, so we can use the eigenvalues of M_x to label the bands on the two planes. That is, the DT2, DT3 and A1, A2 bands are forbidden by mirror symmetry to cross each other.[38]

To elucidate the distribution details of the Dirac nodes in whole BZ, we further constructed a tight-binding model (TB) based on the maximum local Wannier function. As shown in Figure 4a, the Dirac nodes form two horseshoe-like "U" curves on the $k_x = 0$ plane of BZ. That is to say, ABW-Ge_4 is actually a nodal-line semimetal rather than a Dirac nodal-point semimetal.

From the shape and position of the nodes, one can see that the two nodal lines are part of a complete closed ring, residing at the boundary of BZ. To prove this, we further calculated the three-dimensional band structure on an expanded area beyond the first BZ. As shown in Figure 4b, we confirm that the two horseshoe nodal lines indeed form a closed ring. In this sense, ABW-Ge_4 should be a nodal-ring semimetal without SOC.

To explore the transport properties of the Dirac linear dispersion, we examine the Fermi velocities in different momentum directions near the Dirac points as shown in Figure 5a. By constructing a θ and φ spherical coordinate system with N1/N2 as the origin point, the band structure along 7500 $\boldsymbol{k}$ paths through the nodal points N1/N2 is calculated; the Fermi velocities, defined as $\hbar v_F \approx \mathrm{d}E(k)/\mathrm{d}k$, are fitted on the basis of the obtained bands. From Figure 5, one can see that around both N1 and N2, the Fermi velocities of the low-energy linear bands are the direction dependent, exhibiting strong anisotropy, especially near the node. Moreover, the maximum Fermi velocity near the node N2 is 1.3×10^6 m/s, which is even greater than that of the prominent graphene (9.02×10^5, 9.42×10^5 m/s).[39] This is

https://doi.org/10.1021/acsomega.3c02542
ACS Omega 2023, 8, 27231−27237

beneficial for mass-less and non-dissipative ultra-high speed carrier transport applications.

Germanium is a heavy element with *d* orbitals, thus the SOC effect should be considered, which may open a gap at the identified Dirac nodal points and take a topological phase transition to a topological insulator. Figure 6a shows the electronic band structures of ABW-Ge_4 under SOC. One can see that the valence and conductance bands move away from each other and the Dirac points N1 and N2 are fully gapped. Specifically, the opened gap is about 46 meV along the Γ−X path and 99 meV along the G_0−X path, respectively. Owing to the existence of the opened band gap and time inversion symmetry, we further calculated the Z_2 topological invariant according to the evolution of the Wannier charge centers (WCCs)[40] based on the obtained maximum localized Wannier function. Taking an arbitrary horizontal line (e.g., WCC = 0.77 in Figure 6b) as reference, one can see that the number of crossings between the reference line and the evolution of WCC is odd for ABW-Ge_4 under SOC. This indicates that ABW-Ge_4 should be an intrinsic trivial 3D insulator with Z_2 = 1. To provide more visual evidence, we further examined the topological surface states. As shown in Figure 6c, there is a pair of gapless nontrivial surface states (i.e., spin transport channels) traversing across the bulk gap and connecting the conduction and valence bands, which is consistent with the calculated result of Z_2. Therefore, the ABW-Ge_4 system is essentially a 3D topological insulator. Considering the compatibility with traditional semiconductor materials, it is reasonable to believe that ABW-Ge_4 may be promising in future microelectronic topological devices.

4. CONCLUSIONS

In summary, a new Ge allotrope ABW-Ge_4 is defined based on the first-principles calculations. Its stability, electronic properties, and topological properties are systematically studied. The results show that ABW-Ge_4 is a stable topological nodal-line semimetal without SOC, holding many desirable properties: (i) it has excellent dynamic, thermal, and mechanical stability; (ii) there exist two topological nodal lines protected by M_x mirror symmetry, which can be connected into a ring in the Brillouin zone; (iii) strongly anisotropic electron transport characteristics near the N1 and N2 nodes have been confirmed by the calculation of Fermi velocities along different $\boldsymbol{k}$ orientations, and it is found that the maximum Fermi velocity is even larger than that of graphene; and (iv) the electronic band structures of ABW-Ge_4 under SOC indicate that the valence and conductance bands move away from each other and it is fully gapped along the whole high-symmetry direction; ABW-Ge_4 under SOC will be converted into a topological insulator. Our findings establish a new member of topological material in the Group-IV elements. The results of quantum-phase transition from a nodal-line semimetal into a topological insulator as a result of SOC may be widely used in the field of microelectronic devices, due to the compatibility with traditional semiconductor materials.

ASSOCIATED CONTENT

Supporting Information

The Supporting Information is available free of charge at https://pubs.acs.org/doi/10.1021/acsomega.3c02542.

Structural stability of ABW-Ge_4 under spin−orbit coupling (SOC) (PDF)

AUTHOR INFORMATION

Corresponding Author

Xin Cui − *School of Physical Science and Technology, Inner Mongolia University, Hohhot 010021, China;* orcid.org/0000-0002-6858-4482; Phone: +8613204711862; Email: pycuixin@imu.edu.cn

Authors

Yuxin Zou − *School of Physical Science and Technology, Inner Mongolia University, Hohhot 010021, China*

Ningjun Wu − *School of Physical Science and Technology, Inner Mongolia University, Hohhot 010021, China*

Tielei Song − *School of Physical Science and Technology, Inner Mongolia University, Hohhot 010021, China*

Zhifeng Liu − *School of Physical Science and Technology, Inner Mongolia University, Hohhot 010021, China;* orcid.org/0000-0002-8151-6839

Complete contact information is available at: https://pubs.acs.org/10.1021/acsomega.3c02542

Notes

The authors declare no competing financial interest.

ACKNOWLEDGMENTS

This work is supported by the National Natural Science Foundation of China (12264033 and 11964023) and the Natural Science Foundation of Inner Mongolia Autonomous Region (2021JQ-001).

REFERENCES

(1) Saleev, V. A.; Shipilova, A. V.; Proserpio, D. M.; Fadda, G. Ab Initio Study of New sp^3 Silicon and Germanium Allotropes Predicted from the Zeolite Topologies. *Eur. Phys. J. B* **2017**, *90*, 150.

(2) Kong, W.; Xiao, X.; Qin, Z.; Zhan, F.; Wang, R.; Gan, L. Y.; Wei, J.; Fan, J.; Wu, X. Grain Boundaries Induced a Class of Carbon Allotropes with Dirac Fermions. *J. Phys. Chem. C* **2022**, *126*, 12972−12976.

(3) Ding, Y.; Huang, W.; Chang, Y.; Song, Y.; Chen, G. A Novel Two-Dimensional Allotrope of Silicon Grown on Al (111): A Case Study of the Interface Effect. *J. Phys. Chem. C* **2022**, *126*, 21482−21495.

(4) Gorkan, T.; Ozdemir, I.; Bakir, M. Y.; Ersan, F.; Gökoğlu, G.; Aktürk, E.; Ciraci, S. Novel Metallic Clathrates of Group-IV Elements and Their Compounds in a Dense Hexagonal Lattice. *J. Phys. Chem. C* **2019**, *123*, 15330−15338.

(5) Liu, Z.; Xin, H.; Fu, L.; Liu, Y.; Song, T.; Cui, X.; Zhao, G.; Zhao, J. All-Silicon Topological Semimetals with Closed Nodal Line. *J. Phys. Chem. Lett.* **2019**, *10*, 244−250.

(6) Kasper, E.; Oehme, M.; Lupaca-Schomber, J. High Ge Content SiGe alloys: Doping and Contact Formation. *ECS Trans.* **2008**, *16*, 893−904.

(7) Menoni, C. S.; Hu, J. Z.; Spain, I. L. Germanium at High Pressures. *Phys. Rev. B* **1986**, *34*, 362−368.

(8) Nelmes, R. J.; Liu, H.; Belmonte, S. A.; Loveday, J. S.; McMahon, M. I.; Allan, D. R.; Häusermann, D.; Hanfland, M. Imma Phase of Germanium at ∼ 80 GPa. *Phys. Rev. B* **1996**, *53*, R2907−R2909.

(9) Takemura, K.; Schwarz, U.; Syassen, K.; Hanfland, M.; Christensen, N. E.; Novikov, D. L.; Loa, I. High-Pressure cmca and hcp Phases of Germanium. *Phys. Rev. B* **2000**, *62*, R10603−R10606.

(10) Vohra, Y. K.; Brister, K. E.; Desgreniers, S.; Ruoff, A. L.; Chang, K. J.; Cohen, M. L. Phase Transition Studies of Germanium to 1.25 Mbar. *Phys. Rev. Lett.* **1986**, *56*, 1944−1947.

(11) Kiefer, F.; Karttunen, A. J.; Döblinger, M.; Fässler, T. F. Bulk Synthesis and Structure of a Microcrystalline Allotrope of Germanium (m-allo-Ge). *Chem. Mater.* **2011**, *23*, 4578−4586.

(12) Zhao, Z.; Zhang, H.; Kim, D. Y.; Hu, W.; Bullock, E. S.; Strobel, T. A. Properties of the Exotic Metastable ST12 Germanium Allotrope. *Nat. Commun.* **2017**, *8*, No. 13909.
(13) Tang, Z.; Litvinchuk, A. P.; Gooch, M.; Guloy, A. M. Narrow Gap Semiconducting Germanium Allotrope from the Oxidation of a Layered Zintl Phase in Ionic Liquids. *J. Am. Chem. Soc.* **2018**, *140*, 6785−6788.
(14) Nguyen, M. C.; Zhao, X.; Wang, C. Z.; Ho, K. M. Sp^3-Hybridized Framework Structure of Group-14 Elements Discovered by Genetic Algorithm. *Phys. Rev. B* **2014**, *89*, No. 184112.
(15) Cao, W.; Tang, P.; Zhang, S. C.; Duan, W.; Rubio, A. Stable Dirac Semimetal in the Allotropes of Group-IV Elements. *Phys. Rev. B* **2016**, *93*, No. 241117.
(16) Wang, Z.; Sun, Y.; Chen, X. Q.; Franchini, C.; Xu, G.; Weng, H.; Dai, X.; Fang, Z. Dirac Semimetal and Topological Phase Transitions in A_3Bi (A = Na, K, Rb). *Phys. Rev. B* **2012**, *85*, No. 195320.
(17) Wang, Z.; Weng, H.; Wu, Q.; Dai, X.; Fang, Z. Three-Dimensional Dirac Semimetal and Quantum Transport in Cd_3As_2. *Phys. Rev. B* **2013**, *88*, No. 125427.
(18) Liu, Z. K.; Zhou, B.; Zhang, Y.; Wang, Z. J.; Weng, H. M.; Prabhakaran, D.; Mo, S. K.; Shen, Z. X.; Fang, Z.; Dai, X.; Hussain, Z.; Chen, Y. L. Discovery of a Three-Dimensional Topological Dirac Semimetal, Na_3Bi. *Science* **2014**, *343*, 864−867.
(19) Gao, H.; Venderbos, J. W. F.; Kim, Y.; Rappe, A. M. Topological Semimetals from First Principles. *Annu. Rev. Mater. Res.* **2019**, *49*, 153−183.
(20) Wan, X.; Turner, A. M.; Vishwanath, A.; Savrasov, S. Y. Topological Semimetal and Fermi-Arc Surface States in the Electronic Structure of Pyrochlore Iridates. *Phys. Rev. B* **2011**, *83*, No. 205101.
(21) Xu, G.; Weng, H.; Wang, Z.; Dai, X.; Fang, Z. Chern Semimetal and the Quantized Anomalous Hall Effect in $HgCr_2Se_4$. *Phys. Rev. Lett.* **2011**, *107*, No. 186806.
(22) Li, X. P.; Deng, K.; Fu, B.; Li, Y. K.; Ma, D. S.; Han, J. F.; Zhou, J.; Zhou, S.; Yao, Y. Type-III Weyl Semimetals: $(TaSe_4)_2I$. *Phys. Rev. B* **2021**, *103*, No. L081402.
(23) Hořava, P. Stability of Fermi Surfaces and *K* theory. *Phys. Rev. Lett.* **2005**, *95*, No. 016405.
(24) Burkov, A. A.; Hook, M. D.; Balents, L. Topological Nodal Semimetals. *Phys. Rev. B* **2011**, *84*, No. 235126.
(25) Abramovich, S.; Dutta, D.; Rizza, C.; Santoro, S.; Aquino, M.; Cupolillo, A.; Occhiuzzi, J.; Russa, M. F. L.; Ghosh, B.; Farias, D.; Locatelli, A.; Boukhvalov, D. W.; Agarwal, A.; Curcio, E.; Sadan, M. B.; Politano, A. NiSe and CoSe Topological Nodal-Line Semimetals: A Sustainable Platform for Efficient Thermoplasmonics and Solar-Driven Photothermal Membrane Distillation. *Small* **2022**, *18*, No. 2201473.
(26) Wang, Z.; Liu, D.; Teo, H. T.; Wang, Q.; Xue, H.; Zhang, B. Higher-Order Dirac Semimetal in a Photonic Crystal. *Phys. Rev. B* **2022**, *105*, No. L060101.
(27) Weng, H.; Liang, Y.; Xu, Q.; Yu, R.; Fang, Z.; Dai, X.; Kawazoe, Y. Topological Node-Line Semimetal in Three-Dimensional Graphene Networks. *Phys. Rev. B* **2015**, *92*, No. 045108.
(28) Huang, H.; Liu, J.; Vanderbilt, D.; Duan, W. Topological nodal-line semimetals in alkaline-earth stannides, germanides, and silicides. *Phys. Rev. B* **2016**, *93*, No. 201114.
(29) Zhu, Z.; Li, M.; Li, J. Topological semimetal to insulator quantum phase transition in the Zintl compounds Ba_2X (X = Si,Ge). *Phys. Rev. B* **2016**, *94*, No. 155121.
(30) Kohn, W.; Sham, L. J. Self-Consistent Equations Including Exchange and Correlation Effects. *Phys. Rev.* **1965**, *140*, A1133−A1138.
(31) Kresse, G.; Joubert, D. From Ultrasoft Pseudopotentials to the Projector Augmented-Wave Method. *Phys. Rev. B* **1999**, *59*, 1758−1775.
(32) Kresse, G.; Furthmüller, J. Efficient Iterative Schemes for Ab Initio Total-Energy Calculations Using a Plane-Wave Basis Set. *Phys. Rev. B* **1996**, *54*, 11169−11186.
(33) Perdew, J. P.; Burke, K.; Ernzerhof, M. Generalized Gradient Approximation Made Simple. *Phys. Rev. Lett.* **1996**, *77*, 3865−3868.
(34) Politzer, P.; Murray, J. S. The Hellmann-Feynman Theorem: A Perspective. *J. Mol. Model.* **2018**, *24*, 266.
(35) Togo, A.; Tanaka, I. First Principles Phonon Calculations in Materials Science. *Scr. Mater.* **2015**, *108*, 1−5.
(36) Wu, Q. S.; Zhang, S. N.; Song, H. F.; Troyer, M.; Soluyanov, A. A. WannierTools: An Open-Source Software Package for Novel Topological Materials. *Comput. Phys. Commun.* **2018**, *224*, 405−416.
(37) Souza, I.; Marzari, N.; Vanderbilt, D. Maximally Localized Wannier Functions for Entangled Energy Bands. *Phys. Rev. B* **2001**, *65*, No. 035109.
(38) Fang, C.; Weng, H.; Dai, X.; Fang, Z. Topological Nodal Line Semimetals. *Chin. Phys. B* **2016**, *25*, No. 117106.
(39) Zhang, X.; Wang, A.; Zhao, M. Spin-Gapless Semiconducting Graphitic Carbon Nitrides: A Theoretical Design from First Principles. *Carbon* **2015**, *84*, 1−8.
(40) Soluyanov, A. A.; Vanderbilt, D. Computing topological invariants without inversion symmetry. *Phys. Rev. B* **2011**, *83*, No. 235401.

https://doi.org/10.1021/acsomega.3c02542
ACS Omega 2023, 8, 27231−27237